NANO LETTERS

pubs.acs.org/NanoLett

Plasmonic Nanofocusing in a Dielectric Wedge

Ewold Verhagen,*,† L. (Kobus) Kuipers, and Albert Polman

Center for Nanophotonics, FOM Institute for Atomic and Molecular Physics (AMOLF), Science Park 104, 1098 XG, Amsterdam, The Netherlands

ABSTRACT We show that surface plasmon polaritons (SPPs) can be concentrated to subwavelength dimensions in a nanoscale dielectric wedge on a metal substrate. An adiabatic model explains how SPPs propagating on a Ag substrate covered with a thin Si film of slowly increasing thickness become highly confined inside the Si layer. Simulations predict strong subwavelength focusing near the surface plasmon resonance frequency. Unlike alternative strategies, this method does not require the nanoscale shaping of metal surfaces.

KEYWORDS Surface plasmons, nanofocusing, field enhancement, tapered waveguide

Surface plasmon polaritons (SPPs), evanescent surface waves propagating along the interface between a metal and a dielectric, have been suggested as a means to concentrate and control light at subwavelength scales.[1−3] The enhanced fields associated with SPPs can be exploited for sensing and spectroscopy as well as subwavelength photonic circuitry. Because the SPP wavevector is larger than that of light in the bounding dielectric, SPPs can be focused more strongly than light in the plane in which they propagate. Moreover, an increase of the wavevector leads to a decrease of the evanescent extent of the SPP wave normal to the metal surface, as the wavevector component in that direction (k_z) is connected to the wavevector k_x along the direction of propagation $\hat{\mathbf{x}}$ through $k_z^2 = \varepsilon_d k_0^2 - k_x^2$, where ε_d is the relative permittivity of the dielectric. However, on a smooth metal surface the wavevector k_x is only significantly larger than the wavevector of light in the bounding dielectric when the refractive index of the dielectric is high, the losses of the metal are low, and the optical frequency is close to the surface plasmon resonance frequency

$$\omega_{sp} = \omega_p/\sqrt{1 + \varepsilon_d}$$

In principle, one could think of manipulating SPPs excited at the interface of a metal with a high-index dielectric near the surface plasmon resonance frequency to focus light on small length scales. But under those conditions the imaginary part k_x'' of the wavevector $k_x = k_x' + ik_x''$ becomes large, limiting propagation to impractically short lengths. Most designs that aim to achieve plasmonic nanofocusing, both theoretically proposed[4−6] and experimentally demonstrated,[7−13] therefore rely on a geometry that differs from a flat metal surface. In general, a SPP mode on a metallic waveguide of which the geometry is gradually modified can adiabatically transform while it propagates along the waveguide. If the waveguide supports a mode that becomes more strongly confined and that does not exhibit cutoff when the waveguide size is decreased, this mode can be used to achieve nanofocusing. Geometries that support such modes are metal cones,[4,14−16] wedges,[6,17,18] and tapered gaps.[5,19,20] Nanofocusing is achieved at a sharp extremity of such a waveguide. The size of the extremity determines the size to which light can be ultimately concentrated. The focusing is therefore limited by the fabrication quality of the nanoscale metal surfaces.

In this work, we apply the concept of a gradual transformation of a SPP mode in a design in which only the dielectric environment outside a metal surface is varied along the waveguide. SPPs propagating on a smooth metal substrate covered with a thin dielectric film become strongly confined when the dielectric film thickness increases.[21] We show in simulations that SPPs concentrate in a subwavelength focus at a specific position on a dielectric wedge on a Ag substrate when they propagate away from the end of the wedge. In contrast to alternative designs, the nanofocusing in this structure is not localized at a sharp extremity. The properties of the constitutive materials play an important role in the focusing, as it occurs most strongly at the surface plasmon resonance frequency ω_{sp}. We explain the effect in terms of the modes of the waveguide and show that intensity enhancements up to a factor 180 can be reached.

The system of interest is a dielectric wedge on a Ag substrate, which is invariant in the y direction and has a thickness $d(x)$ that increases along the x direction. We consider propagation of TM waves in the x direction. To understand the focusing mechanism, we treat the wedge as a tapered waveguide that varies slowly along x, such that at each position x the transverse z dependence of the field can be described by the field of a mode propagating in an infinitely long waveguide with constant thickness $d(x)$. Figure

* To whom correspondence should be addressed, verhagen@amolf.nl.

† Present address: École Polytechnique Fédérale de Lausanne (EPFL), CH 1015, Lausanne, Switzerland.

Received for review: 06/16/2010
Published on Web: 00/00/0000

DOI: 10.1021/nl102120p | *Nano Lett.* **XXXX,** *xxx,* 000–000

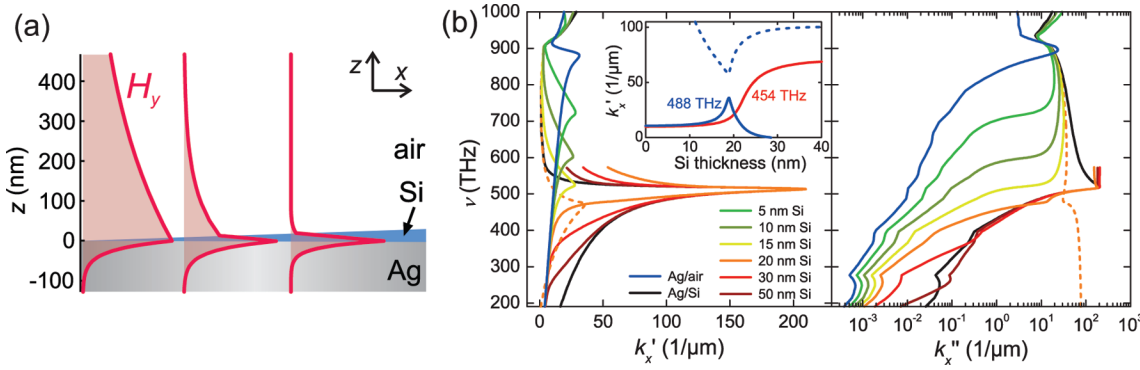

FIGURE 1. (a) SPPs on a metal surface covered with a dielectric film get strongly confined as the film thickness is reduced. The H_y mode profiles of SPPs are calculated for a free-space wavelength of 628 nm on a Ag substrate covered with an infinitely extended Si film of 0, 15, and 20 nm thickness, from left to right. (b) Dispersion curves of SPPs on a thin Si film on Ag, for different Si thicknesses. Real (k_x') and imaginary (k_x'') parts of k_x are displayed. The blue and black curves show the dispersion curves for single Ag/air and Ag/Si interfaces, respectively. For finite Si thickness, the modes resemble SPPs at a Ag/air interface for low frequencies while tending toward the dispersion of SPPs at a Ag/Si interface close to ω_{sp}. The dashed curve shows the dispersion of a second mode for 20 nm, which can play a role in the mode transformation for relatively large frequencies. The inset shows the evolution of k_x' as a function of Si thickness for two frequencies. For 488 THz, the mode that exhibits the largest wavevectors, which cannot be reached adiabatically, is shown as a dashed curve.

1a shows the H_y field profiles of SPP modes guided by a Ag surface covered with a thin Si film of varying thickness, calculated for a free-space wavelength of 628 nm by solving the dispersion relation for a three-layer slab waveguide geometry.[22] Experimentally obtained optical constants of Ag are used,[23] and the refractive index of the Si film is taken as $n = 3.85$. For now, dispersion and absorption in Si are neglected as they are much smaller than in the metal to focus our attention on plasmonic effects only. As Figure 1a shows, a SPP wave that is only moderately confined at a Ag/air interface becomes strongly confined inside the dielectric as d is increased to ~20 nm. The confinement can be explained by considering the dispersion curves of SPPs for varying Si thickness, displayed in Figure 1b. The blue and black curves represent the SPP dispersion at a single Ag/air or Ag/Si interface, respectively. Clearly, the higher permittivity of Si shifts the surface plasmon resonance frequency ω_{sp} (which we define as the frequency for which k_x' is maximal) to a smaller frequency (514 THz), and in principle allows very large wavevectors to be reached near that frequency. The presence of material losses limits the maximum value of k_x' and causes the losses k_x'' to be high for frequencies close to ω_{sp}.

The dispersion curves of SPPs on a very thin (<20 nm) Si film follow those of SPPs on a Ag/air interface closely for most frequencies. As the film thickness increases, the effective surface plasmon resonance can be observed to shift to lower frequencies, approaching the value of ω_{sp} for a single Ag/Si interface. We note that for these small thicknesses SPPs with large wavevectors and negative phase velocity also exist.[22,24,25] For larger Si thicknesses, the dispersion curves approach that of Ag/air SPPs only for small frequencies. Closer to ω_{sp}, the SPP wavevector is similar to that on a Ag/Si interface. The mode makes a transition from being guided predominantly in air to being confined within the Si film as the frequency increases.[26]

Similar behavior will occur when the frequency is kept fixed and the dielectric thickness is continuously increased.[21] This is plotted in the inset of Figure 1b. For a frequency of 454 THz (somewhat smaller than ω_{sp}) k_x changes around a critical thickness of 20 nm from the value for a Ag/air interface to the value for a Ag/Si interface. As a result a SPP mode on a Si wedge on Ag propagating along the direction of increasing Si thickness transforms to a SPP mode that is highly confined in the Si film. Because the losses increase in conjunction with this transformation, the SPPs will not propagate far once they are fully confined in the Si film. The propagation length L_{SPP} reduces to ~200 nm. Nonetheless, the compression could cause a significant field enhancement in a subwavelength volume if it occurs rapidly enough.

One would naively expect the desired effect to be maximal for frequencies closer to ω_{sp}, since the largest wavevectors can be reached there. However, as can be seen in the inset of Figure 1b, for a frequency of 488 THz k_x' first reaches a maximum as the thickness increases, after which it diminishes again. The mode transforms to a wave that is overdamped (evanescent) in the x direction,[21] of which the dispersion curve is plotted for a Si thickness of 20 nm as the dashed line in Figure 1b. Higher order mode coupling, evidenced by an anticrossing in the inset of Figure 1b, prohibits transformation to the mode with the highest possible value of k_x' (the dashed curve in the inset). Nonetheless, we will show that the modes that do get excited can still be responsible for strong field enhancements at the critical thickness, provided the thickness is varied slowly enough.

The mode conversion process is only fully adiabatic when d varies slowly enough for a SPP mode to remain in the corresponding eigenmode while it propagates along the tapered waveguide. Because the eigenvalue k_x can be seen to change rather rapidly with thickness in the inset of Figure 1b, it is likely that adiabaticity can only be reached for

DOI: 10.1021/nl102120p | *Nano Lett.* **XXXX,** *xxx,* 000–000

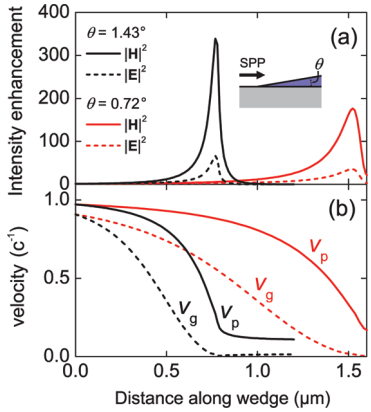

FIGURE 2. (a) Magnetic and electric field intensity enhancements at the Ag/Si interface along Si wedges on Ag, calculated in the eikonal approximation. Two different taper angles θ are considered, and the frequency is 480 THz. The intensities are normalized to the intensity in air at the Ag/air interface at the start of the wedge. (b) Phase and group velocities of the SPPs propagating along the wedges, relative to the speed of light in air.

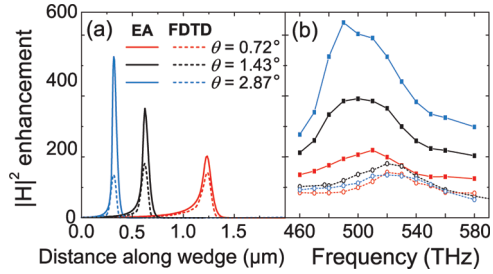

FIGURE 3. Comparison of the $|\mathbf{H}|^2$ intensity enhancements obtained in the eikonal approximation (EA, full curves) and in FDTD simulations (dashed curves). (a) Spatial dependence of the magnetic field intensity enhancement along wedges of three different angles, at a frequency of 520 THz. (b) Spectral dependence of the maximum magnetic field intensity enhancement on the wedges, for the same angles as in (a).

shallow taper angles. In that case, the individual field components Ψ of a wave propagating along $\hat{\mathbf{x}}$ can be written in the eikonal approximation (EA) as[27]

$$\Psi(x, z, t) = A(x)f(x, z)\exp(i\int_0^x k_x(x')\,dx' - i\omega t) \quad (1)$$

where the amplitude $A(x)$ and the mode profile $f(x, z)$ are slowly varying functions in x. Both $f(x, z)$ (the z dependence of the field component Ψ) and $k_x(x)$ are determined from a mode calculation for a planar waveguide of thickness $d(x)$. The energy flux of the mode along the waveguide diminishes only through the calculated mode absorption[4,5]

$$\frac{d}{dx}(\int \mathrm{Re}(\langle S_x\rangle)\,dz) = -2k_x''\int \mathrm{Re}(\langle S_x\rangle)\,dz \quad (2)$$

Here $\langle S_x\rangle = -(1/2)E_zH_y^*$ is the x component of the time-averaged Poynting vector. Hence, in the absence of absorption the energy flux of the mode integrated over the full mode profile remains constant, illustrating that the eikonal approximation neglects scattering to other modes completely and is therefore fully adiabatic. Equation 2 can now be solved to obtain $A(x)$, up to a scaling factor which determines the total power at the start of the waveguide. With that, the field strength along the taper in the eikonal approximation is known for any taper profile $d(x)$.

Figure 2a shows the calculated intensities $|\mathbf{H}|^2$ and $|\mathbf{E}|^2$ along wedges with two different opening angles θ. The intensities are evaluated inside the Si film at the Ag/Si interface, and they are normalized to the intensities at the start of the taper (where $d = 0$) in air at the Ag/air interface. The frequency is 480 THz ($\lambda_0 = 625$ nm). Pronounced maxima are observed at specific positions along the wedge. For both wedges these positions correspond to a local Si thickness of 19 nm. As shown in Figure 2b, the phase velocity v_p approaches a minimum value at that position, after which it remains constant at the value for SPPs at a Ag/Si interface. The group velocity, defined as $v_g = d\omega/dk'$, reaches a value as small as $0.003c$ because the slope of the dispersion curves reduces significantly.[21,26]

After the maximum intensity is reached, the field quickly diminishes because the SPPs are absorbed. Absorption thus also limits the maximum field enhancement that can be obtained. Nevertheless the created field enhancement is significant: intensity enhancements of $|\mathbf{H}|^2$ by a factor 350 are calculated for a taper angle of 1.43°. The enhancement of $|\mathbf{E}|^2$ is five times smaller, which is due to the fact that the requirement of continuity of normal $\mathbf{D}$ fields at the Si/air interface strongly reduces the magnitude of $\mathbf{E}$ inside the Si wedge.

The question remains whether the eikonal approximation presented here is accurate. It is only strictly valid in the limit when $|d(k_x)^{-1}/dx| \ll 1$.[4,5] For $\theta = 1.43°$, $|d(k_x)^{-1}/dx|$ acquires a maximum value of 0.4 at the critical thickness. We therefore additionally perform two-dimensional finite-difference time-domain (FDTD) simulations to take into account scattering into reflected and free-space modes and to quantify the field enhancement.[28] At one of the simulation boundaries a SPP mode on a Ag/air interface is launched with a fixed frequency. A different simulation is performed for every frequency, where a Drude model is locally fitted to experimentally obtained optical constants of Ag.[23] The mesh size near the Ag interface is 0.5 nm, and perfectly matched layers are used as simulation boundaries. The complex fields are recorded at a time of 300 fs, at which time the simulation has reached steady state. The SPPs propagate onto the metal surface with a Si wedge ($n = 3.85$). Figure 3a shows the intensity enhancement of $|\mathbf{H}|^2$ in Si at the Ag/Si interface normalized to the value of $|\mathbf{H}|^2$ in air at the start of the waveguide, for both the eikonal approximation and the FDTD simulations. The excitation frequency is 520 THz ($\lambda_0 = 577$ nm). Both the position and the shape of the

DOI: 10.1021/nl102120p | *Nano Lett.* **XXXX,** *xxx,* 000–000

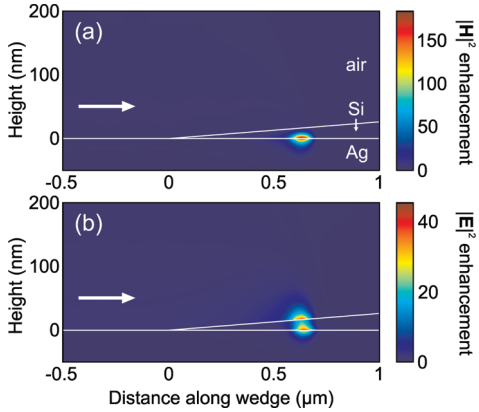

FIGURE 4. Two-dimensional maps of the magnetic (a) and electric (b) field intensity enhancement in a Si wedge on glass with an taper angle of 1.43°, at a frequency of 520 THz ($\lambda_0 = 577$ nm). SPPs are incident from the left, propagating in the direction of the arrow.

intensity distributions obtained from the FDTD simulation agree well with the EA results. The agreement indicates that the explanation of the concentration effect observed in the full-field simulations in terms of a mode transformation in the wedge, as described in the EA, is valid.

As expected, the magnitude of the field enhancement in the FDTD simulations is in general smaller than in the EA, since the latter neglects scattering to all other modes, either reflected or free-space. As can be seen in Figure 3a, for the smallest taper angle of 0.72° the maximum enhancement of $|\mathbf{H}|^2$ in the FDTD simulations is 0.75 times the maximum enhancement in the EA. For larger angles, the deviation is larger, illustrating that adiabaticity breaks down above a taper angle of the order of ~1°. Even though the process is not fully adiabatic, the focusing mechanism still yields a strong field enhancement. A maximum $|\mathbf{H}|^2$ enhancement by a factor 180 is observed for the taper angle of 1.43°. For the largest angles, the deviation from the EA is larger at the right side of the curves; i.e., the field obtained in FDTD starts to diminish after reaching a maximum at a slightly smaller distance along the taper than predicted by the EA. This shows that the breakdown of adiabaticity is most severe very close to the critical thickness.

Figure 3b shows the spectral dependence of the maximum enhancement for the three different taper angles, both for the EA and FDTD methods. Maximum field enhancement is seen to occur at somewhat larger frequencies (520 THz) in the FDTD simulations than in the EA (~500 THz). The fact that this frequency is close to ω_{sp}, which is 514 THz for a Ag/Si interface, shows that the focusing effect relies strongly on the material properties of bulk Si and Ag, which determine the plasmon resonance frequency ω_{sp}.

To estimate the spatial confinement of the concentrated optical energy in the wedge, we plot the field intensity enhancements of $|\mathbf{H}|^2$ and $|\mathbf{E}|^2$ simulated with FDTD at 520 THz ($\lambda_0 = 577$ nm) in Figure 4. The maximum of $|\mathbf{H}|^2$ indeed occurs at the Ag/Si interface, at a very specific position along the wedge. The magnetic intensity is almost fully contained within the Si film at that position, decaying in the z direction to a fraction of $1/e$ of the maximum value at a distance of 10 nm. In the direction along the surface, the full width at half-maximum is 73 nm. This distance is approximately half the wavelength of light in bulk Si, which is 150 nm at this frequency. It demonstrates that the field concentration occurs within a subwavelength length scale in the longitudinal dimension as well. As noted before, the electric field enhancement (displayed in Figure 4b) is not as large as the magnetic field enhancement because we compare the enhanced field inside Si with the field at the start of the wedge in air. In fact, the electric field in the air just outside the wedge is seen to be quite strongly enhanced near the hot spot as well, with approximately the same magnitude as the maximum at the Ag/Si interface. The full width at half-maximum in the x direction (along the wedge) of the region of enhanced field intensity at the air/Si interface is 75 nm, comparable to the longitudinal confinement at the Ag/Si interface.

So far, we have neglected absorption and dispersion in Si. FDTD simulations including absorption and dispersion have shown that the field intensity enhancement amounts to ~70% of the value obtained in the absence of absorption and dispersion for the 1.43° taper angle. The small deviation between the enhancements obtained with and without absorption in Si indicates that the most important factor limiting the maximum field enhancement is in fact absorption in the metal. We note that the concentration effect should also occur when other materials are used. The concentration will be achieved for frequencies near the surface plasmon resonance frequency for that particular metal/dielectric combination. In general, the highest enhancements are expected for metals with relatively low loss, and dielectrics with a relatively high refractive index, as these allow the strongest confinement. On the other hand, it could be true that with a lower-index dielectric it is easier to reach adiabatic performance, as the wavevector does not change as dramatically. The fabrication of ultrathin tapered dielectric films is certainly challenging, but a large range of techniques exists that are especially well suited to shape dielectrics and semiconductors to realize these kinds of structures in practice. By structuring the dielectric in the y direction as well, the SPPs could be focused in that direction too, yielding even higher field enhancements in subwavelength volumes.

We have demonstrated the subwavelength concentration of light in a dielectric wedge on a metal substrate in full-field simulations. The magnetic field intensity of SPPs propagating along a Si wedge on a Ag substrate in the direction of increasing Si thickness is enhanced by a factor of 180 at a well-defined position on the wedge. The mechanism responsible for the concentration effect is the gradual transformation of the SPP mode propagating on a Ag surface covered with a thin Si film of which the thickness slowly increases. At a critical thickness of ~20 nm, the SPPs slow down and

DOI: 10.1021/nl102120p | *Nano Lett.* **XXXX,** *xxx,* 000–000

become fully confined within the Si film, leading to a large buildup of optical energy. Maximum field enhancement is observed for relatively shallow taper angles of ~1°, close to the surface plasmon resonance frequency of SPPs at a Ag/Si interface. The field enhancement in the wedge is maximal at the Ag/Si interface but is still significant at the Si/air surface. It can therefore be of practical interest, for example if one intends to couple emitters or Raman-active molecules dispersed on the surface to the concentrated optical fields. This work presents an alternative route to achieve plasmonic nanofocusing, without the need to fabricate very small metal features. It shows that it is possible to make use of a regime of SPP dispersion that is usually considered impractical because of the associated high losses.

Acknowledgment. This work is part of the Joint Solar Programme (JSP) of the Stichting voor Fundamenteel Onderzoek der Materie (FOM), which is financially supported by the Nederlandse organisatie voor Wetenschappelijk Onderzoek (NWO). The JSP is cofinanced by NWO and Stichting Shell Research. The work is furthermore supported by GCEP.

REFERENCES AND NOTES

(1) Lal, S.; Link, S.; Halas, N. J. *Nat. Photonics* **2007**, *1*, 641–648.
(2) Gramotnev, D. K.; Bozhevolnyi, S. I. *Nat. Photonics* **2010**, *4*, 83–91.
(3) Schuller, J. A.; Barnard, E. S.; Cai, W.; Jun, Y. C.; White, J. S.; Brongersma, M. L. *Nat. Mater.* **2010**, *9*, 193–204.
(4) Stockman, M. I. *Phys. Rev. Lett.* **2004**, *93*, 137404.
(5) Gramotnev, D. K. *J. Appl. Phys.* **2005**, *98*, 104302-11.
(6) Gramotnev, D.; Vernon, K. *Appl. Phys. B: Lasers Opt.* **2007**, *86*, 7–17.
(7) Verhagen, E.; Kuipers, L.; Polman, A. *Nano Lett.* **2007**, *7*, 334–337.
(8) Ropers, C.; Neacsu, C. C.; Elsaesser, T.; Albrecht, M.; Raschke, M. B.; Lienau, C. *Nano Lett.* **2007**, *7*, 2784–2788.
(9) Verhagen, E.; Polman, A.; Kuipers, L. *Opt. Express* **2008**, *16*, 45–57.
(10) Verhagen, E.; Spasenović, M.; Polman, A.; Kuipers, L. *Phys. Rev. Lett.* **2009**, *102*, 203904-4.
(11) Volkov, V. S.; Bozhevolnyi, S. I.; Rodrigo, S. G.; Martín-Moreno, L.; García-Vidal, F. J.; Devaux, E.; Ebbesen, T. W. *Nano Lett.* **2009**, *9*, 1278–1282.
(12) Choi, H.; Pile, D. F.; Nam, S.; Bartal, G.; Zhang, X. *Opt. Express* **2009**, *17*, 7519–7524.
(13) Lindquist, N. C.; Nagpal, P.; Lesuffleur, A.; Norris, D. J.; Oh, S.-H. *Nano Lett.* **2010**, *10*, 1369–1373.
(14) Babadjanyan, A. J.; Margaryan, N. L.; Nerkararyan, K. V. *J. Appl. Phys.* **2000**, *87*, 3785–3788.
(15) Issa, N.; Guckenberger, R. *Plasmonics* **2007**, *2*, 31–37.
(16) Gramotnev, D. K.; Vogel, M. W.; Stockman, M. I. *J. Appl. Phys.* **2008**, *104*, No. 034311−8.
(17) Durach, M.; Rusina, A.; Stockman, M. I.; Nelson, K. *Nano Lett.* **2007**, *7*, 3145–3149.
(18) Vernon, K. C.; Gramotnev, D. K.; Pile, D. F. P. *J. Appl. Phys.* **2007**, *101*, 104312–10.
(19) Pile, D. F. P.; Gramotnev, D. K. *Appl. Phys. Lett.* **2006**, *89*, No. 041111−3.
(20) Gramotnev, D. K.; Pile, D. F. P.; Vogel, M. W.; Zhang, X. *Phys. Rev. B* **2007**, *75*, No. 035431.
(21) Stockman, M. I. *Nano Lett.* **2006**, *6*, 2604–2608.
(22) Dionne, J. A.; Verhagen, E.; Polman, A.; Atwater, H. A. *Opt. Express* **2008**, *16*, 19001–19017.
(23) Johnson, P. B.; Christy, R. W. *Phys. Rev. B* **1972**, *6*, 4370–4379.
(24) Stockman, M. I. *Phys. Rev. Lett.* **2007**, *98*, 177404-4.
(25) Webb-Wood, G.; Kik, P. G. *Appl. Phys. Lett.* **2008**, *92*, 133101-3.
(26) Karalis, A.; Lidorikis, E.; Ibanescu, M.; Joannopoulos, J. D.; Soljačić, M. *Phys. Rev. Lett.* **2005**, *95*, No. 063901.
(27) Born, M. A.; Wolf, E. *Principles of optics*; Pergamon Press: London, New York, Paris, and Los Angeles, 1959; p 558.
(28) Lumerical FDTD Solutions.

DOI: 10.1021/nl102120p | *Nano Lett.* **XXXX,** *xxx,* 000–000